Vertical profiles of aerosol volume from high-spectral-resolution infrared transmission measurements. I. Methodology

Annmarie Eldering, Fredrick W. Irion, Albert Y. Chang, Michael R. Gunson, Franklin P. Mills, and Helen M. Steele

The wavelength-dependent aerosol extinction in the 800–1250-cm^{-1} region has been derived from ATMOS (atmospheric trace molecule spectroscopy) high-spectral-resolution IR transmission measurements. Using models of aerosol and cloud extinction, we have performed weighted nonlinear least-squares fitting to determine the aerosol-volume columns and vertical profiles of stratospheric sulfate aerosol and cirrus cloud volume. Modeled extinction by use of cold-temperature aerosol optical constants for a 70–80% sulfuric-acid–water solution shows good agreement with the measurements, and the derived aerosol volumes for a 1992 occultation are consistent with data from other experiments after the eruption of Mt. Pinatubo. The retrieved sulfuric acid aerosol-volume profiles are insensitive to the aerosol-size distribution and somewhat sensitive to the set of optical constants used. Data from the nonspherical cirrus extinction model agree well with a 1994 mid-latitude measurement indicating the presence of cirrus clouds at the tropopause.

OCIS codes: 280.1100, 290.1090, 010.1100.

1. Introduction

Knowledge of the composition and global distribution of aerosols is needed to improve our understanding of the aerosol's direct effects on Earth's radiation balance and its indirect effects on cloud microphysics and precipitation.[1] Aerosols are also thought to play an important role in heterogeneous chemistry, affecting ozone concentrations.[2] More information about the global distribution and composition of aerosols is essential for assessing and predicting the effect of human activities on a global basis. Remote-sensing instruments are becoming widely discussed as a source of global aerosol information.[3–5]

A. Eldering (annmarie.eldering@jpl.nasa.gov), F. W. Irion, A. Y. Chang, M. R. Gunson, and F. P. Mills are with the Jet Propulsion Laboratory, California Institute of Technology, 4800 Oak Grove Drive, Pasadena, California 91101. A. Eldering, as well as H. M. Steele, is also with the Department of Atmospheric Sciences, University of California at Los Angeles, 405 Hilgard Avenue, Los Angeles, California 90095. H. M. Steele is also with the Department of Geography, California State University at Northridge, 18111 Nordhoff Street, Northridge, California 91330.

Received 5 September 2000; revised manuscript received 1 February 2001.

0003-6935/01/183082-10$15.00/0

In this paper we describe a methodology for retrieving the vertical profiles of aerosol loading from measurements of high-spectral-resolution IR solar occultation. Aerosol composition can also be constrained during this process. The methodology is described in detail here, and an example of the application is presented.

The overall strategy of this technique is to account for transmission reduction due to trace gases and to examine the remaining transmission reduction for the signature of aerosols. Aerosol extinction models are then fit against the continuum spectra to determine quantitatively the aerosol volume present and constrain its composition. The retrieved slant columns are inverted to obtain a vertical profile of aerosol loading.

2. Description of the Method

A. Extraction of the Aerosol Signature

As described in Refs. 6–8, a nonlinear least-squares fitting algorithm can be applied to a measured spectrum to determine the slant-column abundance of gases. This algorithm performs simultaneous adjustments of the gas abundances, the continuum level, and the frequency shift in order to optimize the

fit to the measured spectrum. Examples of spectroscopic fitting can be found in Refs. 9 and 10.

The continuum absorption is the residual after accounting for discrete line absorption by atmospheric gases (including absorption in the far wings of pressure-broadened lines and pressure-induced absorption by N_2 and O_2) and broadly absorbing gases such as chlorofluorocarbons. The term continuum spectrum will refer to this frequency-dependent continuum absorption which we will show can be attributed to extinction by aerosols.

The transmission of solar radiation at a frequency v through an atmosphere containing gases j with absorption coefficients κ_j and number density of the gas g_j along optical slant path x is given by

$$T(v) = K_{\text{meas}}(v)\exp\left\{-\sum_j \left[\int_x \kappa_j(v, x) g_j(x)\mathrm{d}x\right]\right\}. \quad (1)$$

$K_{\text{meas}}(v)$ is the continuum spectrum. Implicit in this separation of terms is that the absorption lines of an individual gas, which are generally less than 0.1 cm^{-1} wide, are not affected in shape by broader absorption features such as those from aerosols. To obtain the continuum spectrum from measurements, it is necessary that the measurements have enough spectral resolution to fit the gas absorption lines accurately. In general, only Fourier transform infrared spectrometers (e.g., atmospheric trace molecule spectroscopy[11] (ATMOS) and Mark-IV[12]) have the required spectral resolution and bandwidth.

We have developed two methods for obtaining continuum spectra from high-spectral-resolution transmission measurements. In the full spectrum method the trace-gas volume-mixing ratio profiles are retrieved first by standard techniques. To calculate the exponential term of the right-hand side of Eq. (1), we then use these trace-gas volume-mixing ratios in a line-by-line forward model for the full spectrum. The ratio of this to the observed transmission gives the continuum spectrum $K_{\text{meas}}(v)$. However, uncertainties in spectroscopic parameters combined with measurement uncertainties can cause a frequency shift that depends on wave number, which makes the full spectrum method impractical. An alternative technique is the spectral window method in which the spectrum is divided into 2-cm^{-1} intervals that are treated individually. Trace gases are retrieved independently within each window, and the continuum is determined for each spectral window. These two techniques result in effectively the same values for the continuum, but the spectral window method has been chosen for routine processing because of its greater simplicity.

The continuum uncertainty σ is the sum of the uncertainties in the fit for every gas present in the spectral window and the uncertainty due to the zero offset error.[13] The summation is done in the customary manner for propagating multivariate uncertainties. In the regions used for this research, the term due to the zero-offset uncertainty generally accounts for more than 90% of the uncertainty in the continuum. The continuum spectra may include absorption by gases that were not fit or were not fit properly in the gas-phase retrieval. However, our results suggest that the continuum spectra are due to the extinction produced by aerosols.

In earlier research, Rinsland *et al.*[14] reported on mid-IR extinction by aerosols in the ATMOS dataset by using an analysis that relied on microwindows free of telluric lines. Our new approach requires only the ability to fit the gas-absorption lines accurately, can be performed over a very large range of frequencies (hundreds of wave numbers), and is easily implemented for routine automated processing.

B. Modeling Transmission through Aerosols

We can define an extinction coefficient per unit particle-number density $b_i(v, x)$ and total aerosol-number density (number of particles per volume of air) $N_i(x)$ of aerosol type i along optical path x. The total aerosol-number density is the integral of the number distribution,

$$N_i = \int_0^\infty \frac{\mathrm{d}N_i}{\mathrm{d}r}\,\mathrm{d}r,$$

where r is the aerosol-particle radius. The modeled aerosol spectrum can be expressed as

$$K_{\text{model}}(v) = \exp\left\{-\sum_i \left[\int_x b_i(v, x) N_i(x)\mathrm{d}x\right]\right\}. \quad (2)$$

For a given aerosol-size distribution at location x, $b_i(v)$ is given by

$$b_i(v) = \frac{\int_0^\infty \pi r^2 Q_i \frac{\mathrm{d}N_i}{\mathrm{d}r}\,\mathrm{d}r}{\int_0^\infty \frac{\mathrm{d}N_i}{\mathrm{d}r}\,\mathrm{d}r}. \quad (3)$$

The Mie efficiency factor Q_i is calculated for a given aerosol composition, which determines the refractive index.

For the retrieval of aerosol volume, we can also define $a_i(v, x)$, the corresponding extinction coefficient per unit aerosol-mixing ratio (volume of aerosol per volume of air), given by

$$a_i(v) = \frac{\int_0^\infty \frac{3}{4r} Q_i \frac{\mathrm{d}V_i}{\mathrm{d}r}\,\mathrm{d}r}{\int_0^\infty \frac{\mathrm{d}V_i}{\mathrm{d}r}\,\mathrm{d}r}, \quad (4)$$

where

$$\frac{\mathrm{d}V_i}{\mathrm{d}r} = \frac{4\pi r^3}{3}\frac{\mathrm{d}N_i}{\mathrm{d}r}.$$

The modeled aerosol spectrum can also be expressed as

$$K_{\text{model}}(v) = \exp\left\{ -\sum_i \left[\int_x a_i(v, x) V_i(x) \mathrm{d}x \right] \right\}. \quad (5)$$

The slant column of the aerosol number of type i is then

$$L_{Ni} = \int_x N_i(x) \mathrm{d}x,$$

and for aerosol volume it is

$$L_{Vi} = \int_x V_i(x) \mathrm{d}x.$$

In the cases in which $a_i(v)$ and $b_i(v)$ can be considered invariant along the slant path and multiple aerosol types are present, Eq. (2) becomes

$$K_{\text{model}}(v) = \prod_i \exp[-a_i(v) L_{Vi}] = \prod_i \exp[-b_i(v) L_{Ni}]. \quad (6)$$

C. Vertical Profiles of Aerosols

An occultation measurement consists of a series of spectra that is taken during a sunrise or sunset where the spectra occur at different tangent heights of the optical path above the Earth. In satellite occultation measurements the geometric slant-path distance x includes contributions from all altitudes along the slant path, and thus a single spectrum cannot be used to derive the vertical profile of $V_i(x)$. A series of spectra at different tangent altitudes is necessary to find the vertical profile. First, an error σ weighted nonlinear least-squares fitting of $K_{\text{model}}(v)$ to $K_{\text{meas}}(v)$ is applied to each continuum spectrum to retrieve the aerosol volume slant column L_{Vi} and an associated slant-column uncertainty. The chi-squared χ^2 of the fit is given by

$$\chi^2 = \sum_{k=1}^{\text{no. of spectral points}} \left[\frac{K_{\text{meas}}(v_k) - K_{\text{model}}(v_k)}{\sigma(v_k)} \right]^2. \quad (7)$$

The set of slant columns and the matrix of slant-path distances are then inverted with a linear equation solver to yield a vertical profile of the aerosol volume and the associated uncertainty.

D. Aerosol Models for Fitting

A wide variety of aerosols are of interest globally and could potentially be included in Eq. (6). These aerosols include sulfuric acid, dust, soot from biomass burning, tropospheric aerosols such as ammonium nitrate and organic aerosols, polar stratospheric clouds, ice clouds, and water droplet clouds. With our aerosol extinction estimation (AXE) program, Mie extinction calculations are conducted at wavelengths between 0.2 and 20 μm by using refractive-index data for sulfuric acid droplets of variable composition,[15–17] ammonium sulfate,[18] nitric acid,[19,20] water,[21] dust,[22] and ternary solutions of water, sulfuric acid, and nitric acid.[23] For ice we used the optical constants of Ref. 24 for the spherical ice model as well as the extinction coefficients from nonspherical scattering models.[25] Yang and *et al*. in their models[25,26] used ray-tracing and geometrical-optics techniques to describe scattering that is due to plates, columns, rosettes, and other typical ice shapes. The AXE model and Yang's extinction data provide the capability to predict extinction for more than half a dozen materials with particle sizes specified by one of a number of distribution functions.

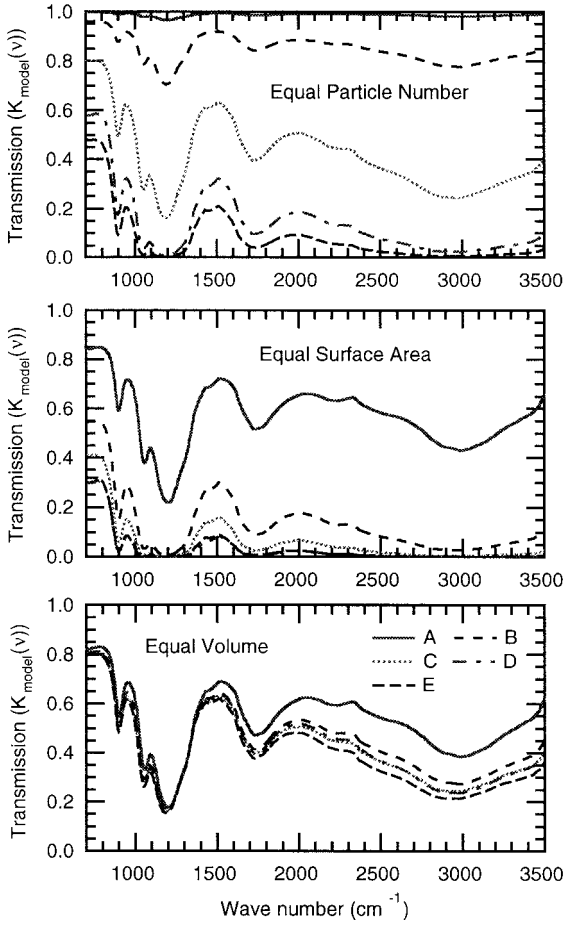

Fig. 1. Transmission for equal particle number, surface area, and particle volume by using five different aerosol-size distributions for stratospheric sulfuric acid. The size distributions are described in more detail in Table 1.

In the IR region the term $a_i(v)$, which transforms extinction to volume, is fairly insensitive to assumptions about the aerosol-size distribution. Figure 1 illustrates the transmission calculated from the extinction coefficient normalized by particle-number density $b_i(v)$, surface-area density, and volume-mixing ratio $a_i(v)$ for five different aerosol-size distributions. For convenience the extinction coefficient normalized by surface-area density will be denoted by $s_i(v)$. The size distributions that were used are described in more detail in Table 1 and were selected as representative of measured size distributions for

Table 1. Representative Size Distributions of Stratospheric Sulfuric Acid Aerosols Used in Fig. 1

Label	Description	Parameters	Conditions
A	Log normal	R_g = 0.07 μm, σ = 1.41 (Ref. 27)	Background
B	Log normal	R_g = 0.08 μm, σ = 2.06 (Ref. 28)	Background
C	Log normal	R_g = 0.18 μm, σ = 1.80 (Ref. 27)	Volcanic
D	Bimodal log normal ($N_{\text{mode 1}}/N_{\text{mode 2}}$ = 0.65)	R_{g1} = 0.14 μm, σ_1 = 1.41 R_{g2} = 0.42 μm, σ_2 = 1.36 (Ref. 27)	Volcanic
E	Bimodal log normal ($N_{\text{mode 1}}/N_{\text{mode 2}}$ = 0.52)	R_{g1} = 0.08 μm, σ_1 = 1.50 R_{g2} = 0.39 μm, σ_2 = 1.50 (Ref. 29)	Volcanic

stratospheric sulfuric acid aerosol (SSAA). The values of $b_i(v)$ and $s_i(v)$ are dependent on the aerosol-size distributions. In contrast, $a_i(v)$ is relatively independent of aerosol size, especially in the 800–1500-cm^{-1} region. Thus the transformation from extinction to volume is valid for a wide range of size distributions.

As a result, information about SSAA mass or volume loading can be retrieved rather accurately, but aerosol-size distributions cannot be retrieved from mid-IR measurements. This was explored in the analysis of the improved stratospheric and mesospheric sounder (ISAMS) data[30] and of Michelson interferometer for passive atmospheric sounding-balloonborne version (MIPAS-B) data.[31] Our analysis for dust, which typically has a mean particle size of 1 or 2 μm, shows that there is significant size influence on $a_i(v)$ in this region as scattering becomes important and extinction is no longer simply proportional to volume. Therefore the retrieval of aerosol-volume loading will be affected by size assumptions for materials that have relatively large particles, such as dust and ice.

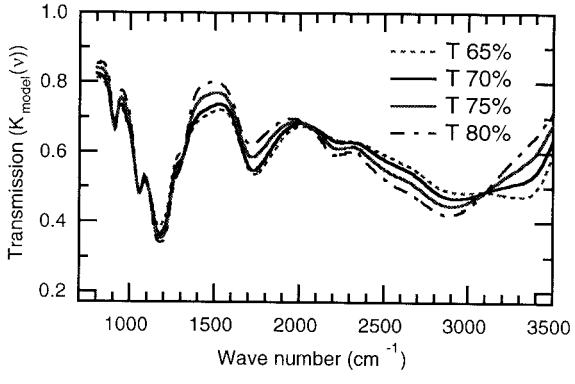

Fig. 2. Transmission for an equal aerosol volume of SSAA with four different compositions. Optical constants from Ref. 16, which were measured at 215 K, are used.

Composition can also affect $a_i(v)$, $s_i(v)$, and $b_i(v)$. Figure 2 shows the transmission calculated from $a_i(v)$ for five different compositions from 65- to 80-wt. % sulfuric acid. These values span the normal range of mid- and low-latitude SSAA composition in the stratosphere.[32] The modeled results in Fig. 2 show strong sensitivity to composition, especially in the absorption band centered at 1200 cm^{-1} and the region from 2500 to 3500 cm^{-1}. Refractive indices are taken from Ref. 19, and the SSAA size distribution from Table 2 is used in the calculation of $a_i(v)$.

Figure 3 shows $b_i(v)$ for four different aerosol materials. Sulfuric acid and ammonium sulfate have distinct spectral patterns in the IR whereas the dust and the ice models show less spectral dependence. In addition the extinction coefficients for ice and dust are approximately one fifth of the magnitude of that for sulfuric acid and ammonium sulfate. Ideally, these strong distinctions could be used to identify types of stratospheric and tropospheric aerosol. Unfortunately, many parts of this spectral regime are inaccessible for aerosol retrievals owing to large gas absorption. Because of the long path length along the line of sight through the atmosphere and the magnitude of their extinction coefficients, limb transmission measurements are able to detect relatively small quantities of aerosols such as sulfuric acid and ammonium sulfate. At the other extreme, cirrus clouds or polar stratospheric clouds encountered along the line of sight, with large values of $b_i(v)$, can cause the signal to fall to its noise limit. However, clouds that are optically thick in the UV or visible can still offer retrieval information in the IR.

Table 2. Selection of Aerosol Descriptions[a]

Material	Source/Location	Size Distribution (all Lognormal)	Optical Constant Data Source (Ref)
Sulfuric acid	Ubiquitous in the stratosphere	R = 0.07 μm, σ = 2.03 (Ref. 27)	17
Ammonium sulfate	Anthropogenic tropospheric aerosol	R = 0.4 μm, σ = 1.8 (Ref. 33)	34
Dust	Windblown and long-range transport from desert areas	R = 1.0 μm, σ = 1.8 (Ref. 35)	22
Ice	Upper tropospheric clouds	R = 2.5 μm, σ = 1.8 (Ref. 25)	24

[a]The IR extinction spectra of these materials are shown in Fig. 3.

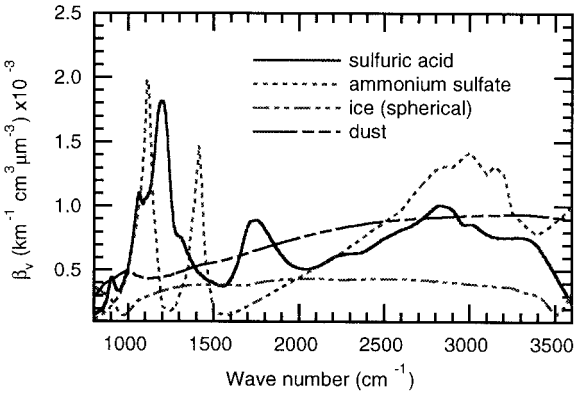

Fig. 3. Mass extinction coefficients per unit aerosol mixing ratio for four different aerosol materials, which are described in Table 2.

3. Application Example

The methodology described here has been applied to data from the ATMOS experiment,[11] and the analysis is applied to data from the Mark-IV instrument.[12] A more extensive report of the results will be set forth in another journal article, and a brief example of the application will be presented here. ATMOS is a high-resolution interferometer that takes measurements from 2.2 to 16 µm with a resolution of 0.01 cm^{-1}. The ATMOS data set was collected from the Space Shuttle in four missions, with data collection lasting from 24 h to 11 days in 1985, 1992, 1993, and 1994. Approximately 350 occultations are available, each containing 50–100 spectra. During a single occultation, spectra are collected through one of six optical bandpass filters that are 600–1600 cm^{-1} wide. The Mark-IV instrument covers 650–5650 cm^{-1} simultaneously through two filters with a spectral resolution of 0.01 cm^{-1}, and measurements were taken from the ground, balloon, and aircraft.

Figure 4 shows a recorded transmission spectrum from an ATMOS measurement at a tangent height of 17 km, the calculated absorption that is due to trace gases, and continuum spectra $K_{\text{meas}}(v)$, which were computed with both the full spectrum method and the spectral window method. The two methods of computing the aerosol continuum show good agreement in shape and overall magnitude. However, the full spectral method has more noise because of frequency shifts that are not properly accounted for. For the study of sulfuric acid aerosols and ice particles, two regions of the IR spectrum were chosen for fitting, 820–990 and 1070–1240 cm^{-1}. These regions contain significant absorption bands for H_2SO_4 and minimal interference from absorption lines that

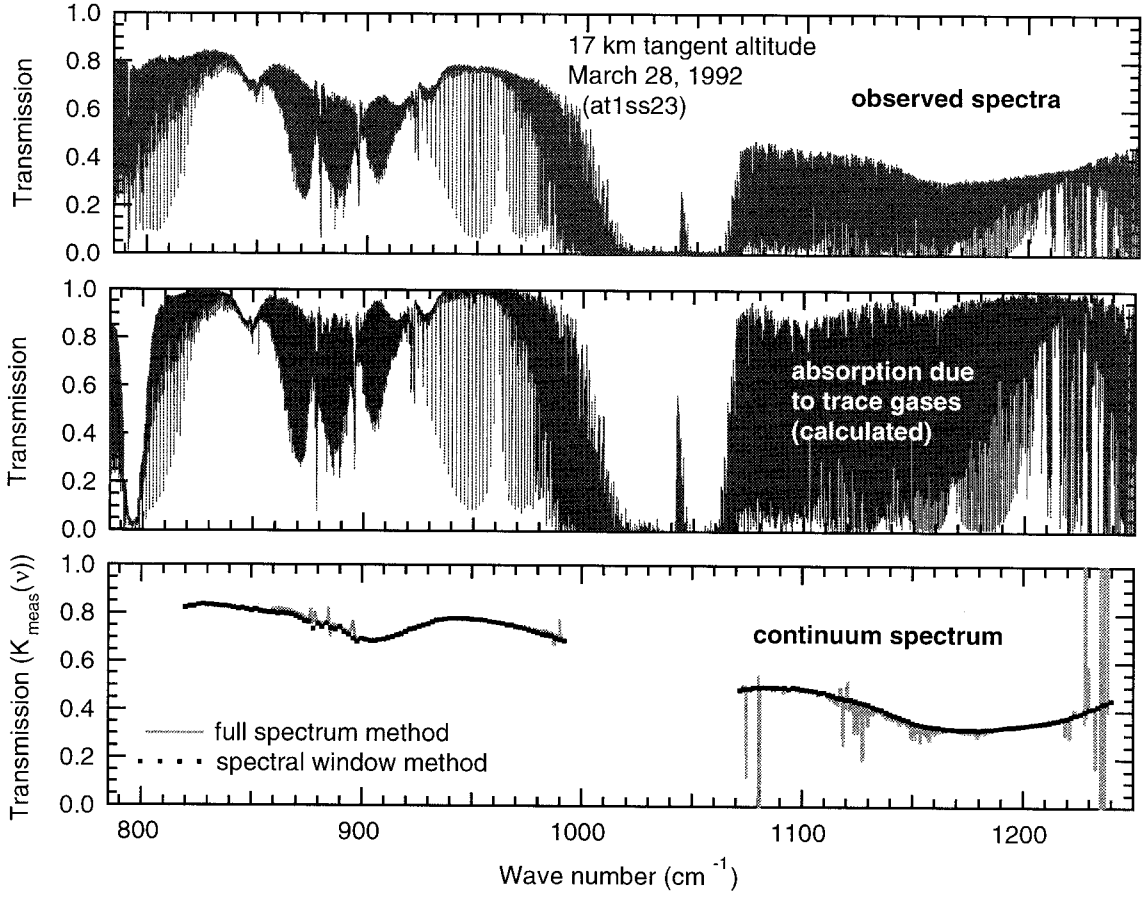

Fig. 4. Measured IR transmission, calculated transmission resulting from the presence of only trace gases, and continuum spectra obtained by two methods, which are described in detail in the text.

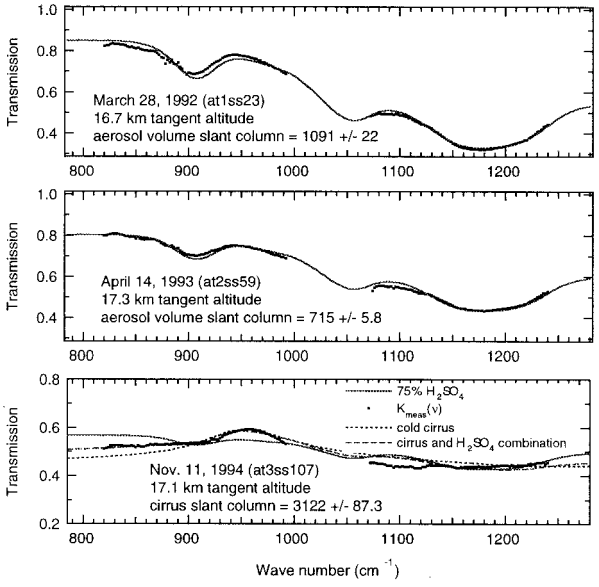

Fig. 5. Continuum spectra and best-fit aerosol models (for SSAA, Ref. 16 refractive indices are used, and the cold cirrus model is from Ref. 25). The locations of the measurements are 45S 41W (at1ss23), 27S 4W (at2ss59) and 41N 187W (at3ss107).

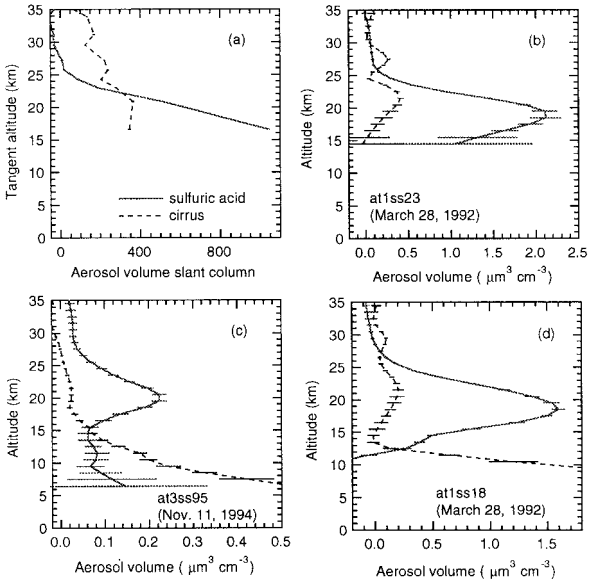

Fig. 6. (a) Volume slant columns (μm^3 cm^{-3} km) and (b) retrieved vertical profiles for ATMOS occultation at1ss23. Vertical profiles that include significant cloud volumes from (c) a 1994 measurement and (d) another 1992 measurement are also shown. The cloud volumes and column have been multiplied by 0.01. The location of at1ss18 was 44S 95E, and at3ss95 was made at 16N 117E.

are due to trace gases. Complete absorption of radiation by ozone around 1040 cm^{-1} prohibits the use of data in that region.

For the calculations presented here, it was assumed that the composition of the aerosol was constant throughout the atmosphere and only the number density varied. This simplifying assumption eliminates the need for a layered atmosphere forward model and greatly simplifies the fitting procedure. Using thermodynamic models[32] and temperature and water-vapor profiles obtained from ATMOS, we can predict that the composition of SSAA is fairly constant and generally between 65% and 80% H_2SO_4 by weight. Various refractive-index data sets for sulfuric-acid aerosols have recently become available, and the sensitivity of a retrieval to these is presented in Section 4. A set of four nonspherical ice extinction spectra[25] (cold cirrus, warm cirrus, cirrus uncinus, and cirrostratus) and a spherical ice extinction spectrum computed by standard Mie theory were considered. Three case studies were carried out—fitting to SSAA only, ice only, and the simultaneous presence of SSAA and ice. The examination of chi-squared values χ^2 showed that, of the ice models, the cold cirrus consistently resulted in the lowest chi-squared values. Therefore only results in which the cold cirrus ice description was used are presented here along with a number of SSAA models.

4. Results

Figure 5 illustrates three continuum spectra from different measurement periods together with the best-fit aerosol models. The upper two figures show the best-fit SSAA-only case and measurements from 1992 and 1993. The increase in transmission and the decrease in slant column from 1992 to 1993 for similar tangent altitudes show the decay of the SSAA after the eruption of Mt. Pinatubo in 1991. The lowest figure shows the detection of a cirrus cloud and all three case studies. The best-fit SSAA-only case results in a chi-squared value of 390 and poor fits from 820 to 890 cm^{-1} and 1070 to 1130 cm^{-1}. The best fit when only the cold cirrus case was used results in a chi-squared value of 207 and poor fits in the same regions, although the error in the 820–890-cm^{-1} region is the opposite sign to that of the SSAA model. The fit from the SSAA and cold cirrus combination case has a chi-squared value of 81, significantly smaller than the chi squared for either single-aerosol case. For the 1992 and the 1993 measurements there is little difference in either the retrieved aerosol-volume slant column or the chi-square values from the SSAA-only and combined SSAA/ice case studies.

As noted in Refs. 14 and 36 the nonlinear response of the HgCdTe detector of ATMOS introduces an unknown transmission scaling factor. To account for this uncertainty, the fitting algorithm uses $\alpha K_{\mathrm{model}}(v)$ rather than $K_{\mathrm{model}}(v)$ and retrieves α along with L_{Vi}. The scaling factor α varies between 1 and 0, allowing the model spectra to be displaced in transmission. This factor takes account of instrumental effects as well as any spectrally independent broad absorber. The retrieved scaling factors for the three spectra shown in Fig. 5 are 0.998, 0.974, and 0.771, indicating little displacement for the SSAA cases. Examination of the whole ATMOS data set shows that offsets smaller than 1 are often required for the lowest two or three tangent altitude spectra.

The aerosol volume slant column and the corre-

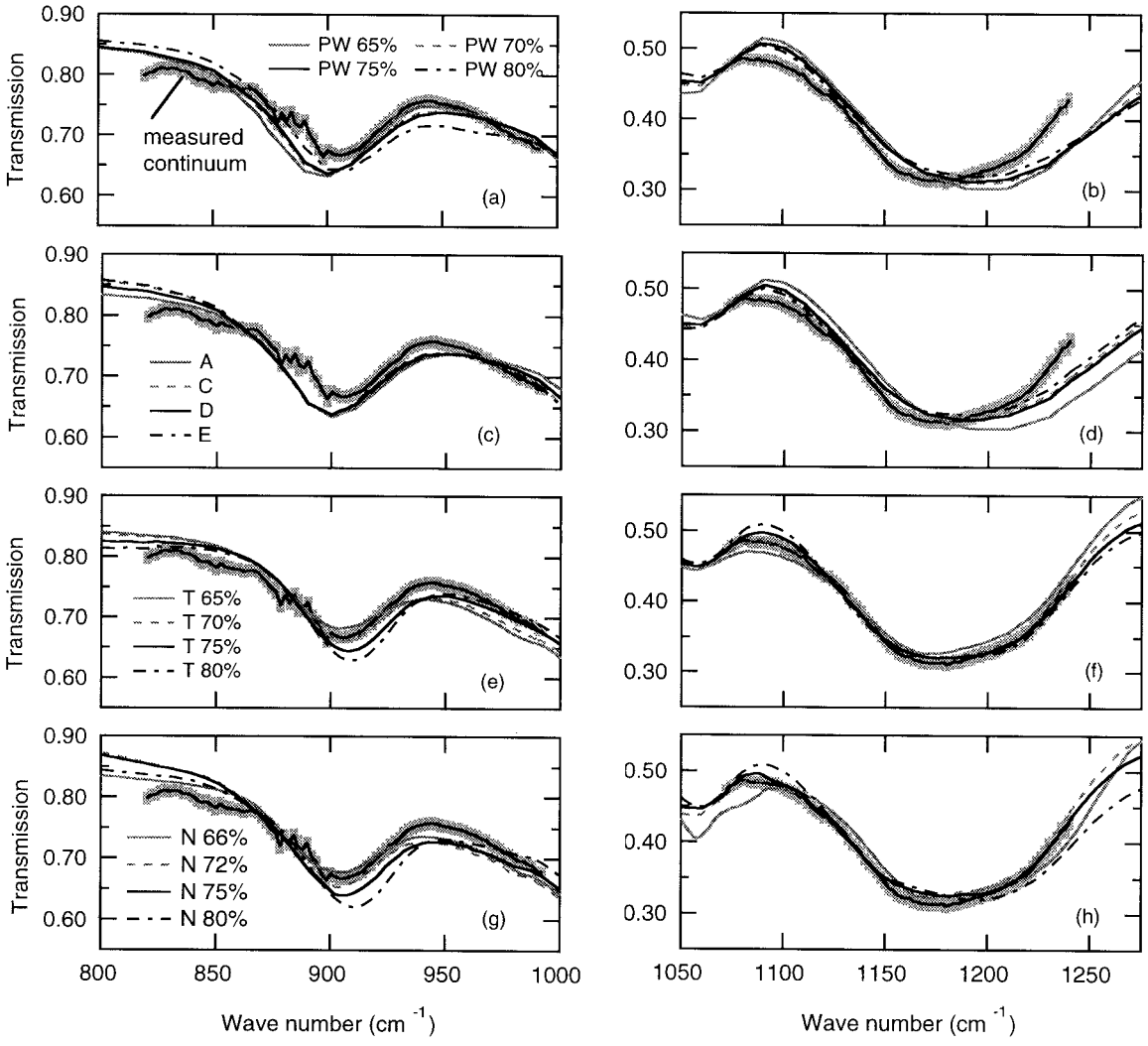

Fig. 7. Continuum spectra and best-fit models for (a), (b), (e)–(h) a range of SSAA composition and (c), (d) size distribution. The refractive indices used are (a)–(d) from Palmer and Williams,[15] (e), (f) from Tisdale *et al.*,[16] and (g), (h) from Niedziela *et al.*[17] The Palmer and Williams measurements were made at 300 K, Tisdale *et al.* at 215 K, and Niedziela *et al.* at 210–240 K. The size distributions used in (c) and (d) are described in Table 1 and use the refractive indices of Palmer and Williams. The left and right figures show two different wave-number regions. Note the change in the transmission scale. The measurement error is shown as gray bars on the continuum spectra.

sponding retrieved vertical profile of the aerosol volume for an ATMOS measurement from 1992 are illustrated in Fig. 6. Two other examples of vertical profiles are shown in the lower figures. Error bars are included on the slant columns and the vertical profiles. The error bar of the vertical profile includes both the uncertainty in the fit of the aerosol model to the continuum spectra and the number and self-consistency of the slant-path measurements that make up the occultation and are inverted to recover the vertical profile. The vertical profiles of the SSAA shown in Fig. 6 illustrate the large difference in the peak concentration of the SSAA between 1992 (1.5–2.0 $\mu m^3\ cm^{-3}$) and 1994 (0.20 $\mu m^3\ cm^{-3}$), consistent with reports of the aerosol volume shortly after the eruption of Mt. Pinatubo[30,37,38] and the decay of the aerosol layer in the following years.[39] In two of the examples, cirrus clouds are evident at tangent altitudes below 15 km. For both of these observations, the tropopause is located at the tangent altitude where the clouds become evident.

The aerosol-size distribution, composition, and refractive-index data combination used in retrieving the aerosol-volume slant columns and profiles shown in Figs. 5 and 6 is only one of many possible combinations. Figure 7 illustrates the sensitivity of our results to these variables. Here the continuum spectrum and the best-fit models for the 17-km tangent altitude measurement of at1ss23 are shown (upper panel, Fig. 5). The two spectral regions used for fitting are shown on separate panels to allow for different transmission scales. Figures 7(a) and 7(b) show best-fit models that use refractive indices from Ref. 15 (Palmer75) for weight percents between 65% and 80%. All the aerosol models use a log-normal distribution with a median radius of 0.07 μm and a

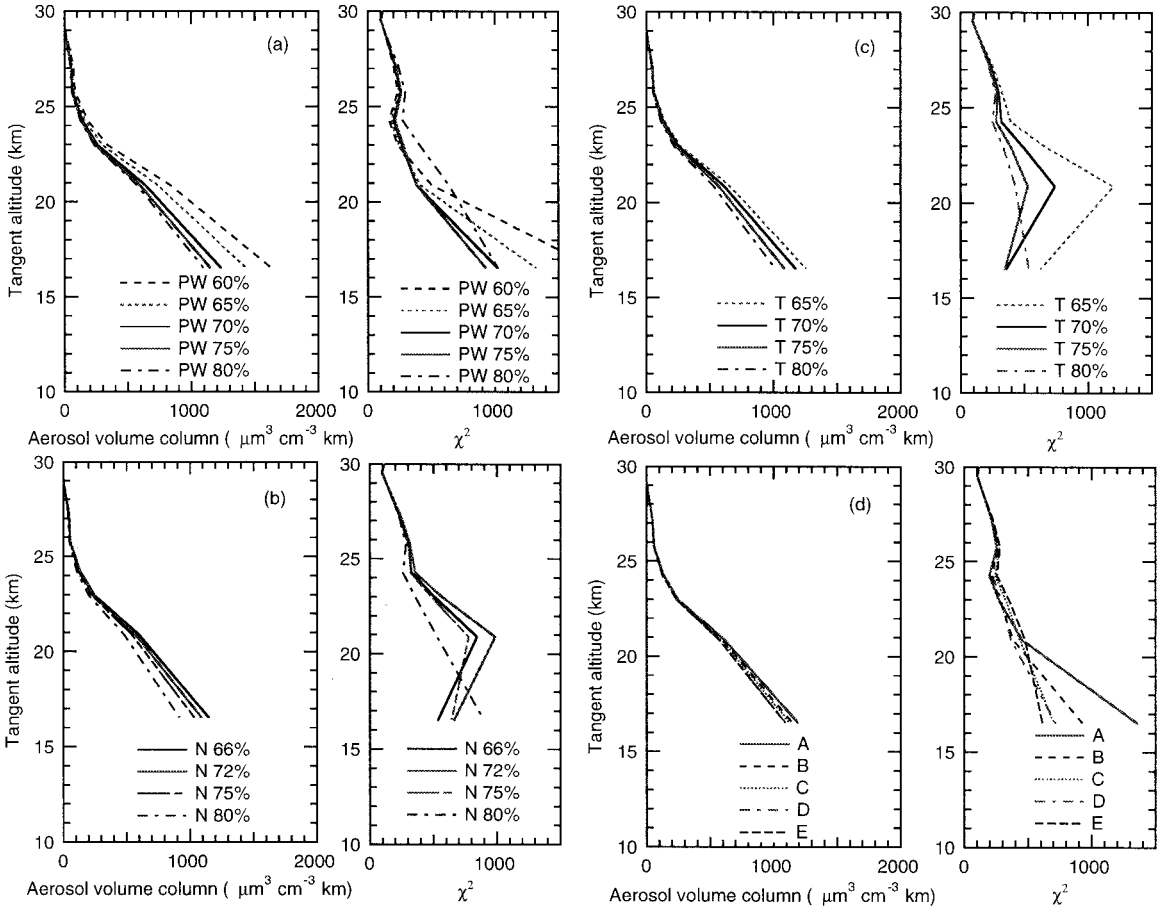

Fig. 8. Aerosol slant columns and χ^2 of the slant columns for a variety of SSAA models. The refractive indices and size distributions are as in Fig. 7.

standard deviation of 2.03 unless stated otherwise. In Figs. 7(c) and 7(d), Palmer75 refractive indices for 75% acid are used with the set of aerosol-size distributions described in Table 1. The Palmer75 data collected at 300 K have been corrected for a lower temperature by application of the Lorentz–Lorenz formula.[32] Figures 7(e) and 7(f) show a similar range of weight percents where the refractive indices at 215 K reported in Ref. 16 are used (Tisdale98). In Figs. 7(g) and 7(h) the refractive-index data reported in Ref. 17 (Niedziela98) are used for a similar range of compositions. The Niedziela98 data include the temperature dependence. A set of measurement data was used that corresponds to the equilibrium sulfuric acid–water solutions for 5×10^{-4} mbar of water.[17] The weight percent–temperature pairs used are 66% at 220 K, 72% at 220 K, 75% at 230 K, and 80% at 240 K. Error bars on the measured continuum are shown as gray bars. The modeled SSAA extinction based on Palmer75 in Figs. 7(a)–7(d) show poor agreement with the ATMOS spectra, as noted in Ref. 14. Most of the composition variation of the Tisdale98 data is in the 900-cm^{-1} region, and the 1050–1250-cm^{-1} data agree well with ATMOS. Neidziela98 data have a wider composition variation, not all of which agree with the ATMOS data. Overall, the 800–900- and 1100–1250-cm^{-1} bands are in better agreement with the new optical constant data, and discrepancies remain in the 900–1000-cm^{-1} region.

In Fig. 8 the aerosol-volume slant column and the χ^2 values as a function of tangent altitude show a quantitative comparison of the different aerosol models. For all sets of refractive-index data, the aerosol models of 70–80% SSAA have the smallest χ^2 values, consistent with the SSAA composition calculated from ATMOS water-vapor temperature and the composition reported in Ref. 36. A more complete and systematic analysis needs to be conducted with the complete ATMOS data set to determine whether a narrow range of SSAA composition or one source of refractive-index data reliably provides a better fit to the observations. The similarity $b_i(v)$ for different size distributions is reflected in the similarity of their retrieved aerosol-volume columns shown in Fig. 8(d) and illustrates the impossibility of using IR extinction or emission measurements to gain aerosol-size distribution information.

These aerosol-volume slant columns were inverted to the vertical aerosol-volume profiles presented in Fig. 9. As expected from the differences in the aerosol-volume column, the aerosol-volume profiles

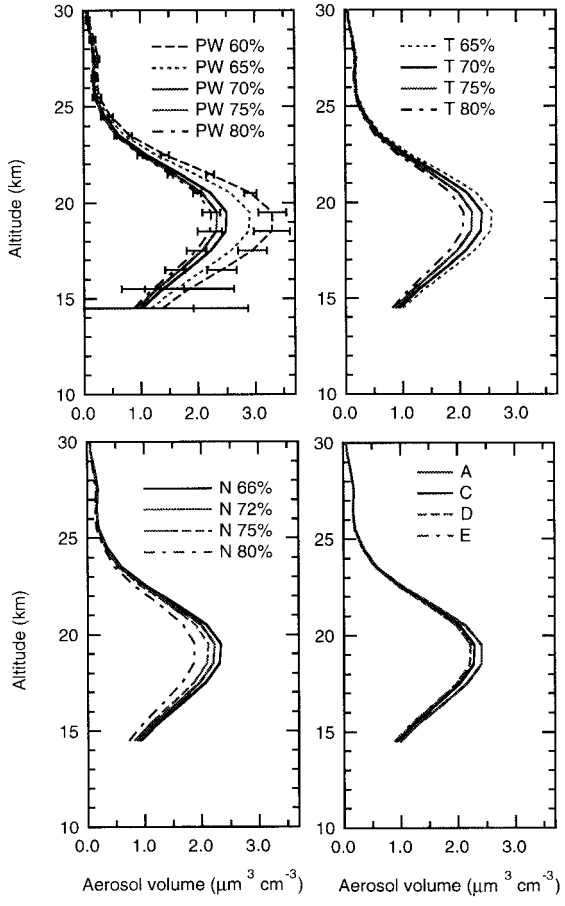

Fig. 9. Vertical profiles of aerosol volume (volume of aerosol per volume of air) for the 28 March 1992 measurement where different sources of optical constant data are used. The refractive indices and size distributions are as described in Fig. 7.

retrieved when refractive indices from Palmer75 were used for low weight percents are larger than those from Tisdale98 or Niedziela98. Error bars are shown only on 60% and 80% SSAA from Palmer75. The relative error of the reported volume is 3.5% at 20 km and 11% at 16 km, and it is essentially the same for all the aerosol models. Again, there is little sensitivity to the aerosol-size distribution, and the volumes are similar to those obtained with the Palmer75 refractive indices for 75% SSAA. Although the differences in aerosol-volume profiles retrieved when Tisdale98 and Niedziela98 are used are not large across the composition shown here, the χ^2 values clearly indicate that the 70% or 75% SSAA models are the best fits. The aerosol volumes retrieved for these compositions agree quite well for the Palmer75, Tisdale98, and Niedziela98 refractive indices.

5. Conclusions

We have described a method for retrieving aerosol profiles from high-spectral-resolution IR transmission measurements. The aerosol signature can be separated from the gas-absorption features and fitted with models. Clear signatures of stratospheric sulfuric acid and cirrus ice clouds have been found in the ATMOS data set. SSAA modeled with a composition of 70–80% has the lowest χ^2 values, consistent with thermodynamic predictions of SSAA composition. There is little sensitivity of retrieved aerosol volume to the assumed size distribution. Optical data from three different sources with temperature dependence typically result in a 20% discrepancy in the peak retrieved volume. Examples of vertical profiles of SSAA and cirrus clouds are shown, reflecting the post-Pinatubo decay in SSAA between 1992 and 1994 and identifying cirrus clouds at the tropopause. In a companion paper, results for the whole of the ATMOS ATLAS (Atmospheric Laboratory for Applications in Science) experiments will be presented along with comparisons of aerosol extinction from cryogenic limb array etalon spectrometer (CLAES) and ISAMS.

Significant funding for this project (A. Eldering, F. P. Mills, and H. M. Steele) was provided by the Caltech President's Fund and NASA contract NAS7-1260, NASA Award NAG5-6396, and NASA New Investigator Grant NAG5-8812. Research at the Jet Propulsion Laboratory was carried out under contract with NASA.

References

1. R. J. Charlson and J. Heintzenberg, eds., *Dahlem Workshop Report on Aerosol Forcing of Climate* (Wiley, New York, 1995).
2. F. J. Dentener, G. R. Carmichael, Y. Zhang, J. Lelieveld, and P. J. Crutzen, "Role of mineral aerosol as a reactive surface in the global troposphere," J. Geophys. Res. **101,** 22869–22889 (1996).
3. Y. J. Kaufman, D. Tanré, H. R. Gordon, T. Nakajima, J. Lenoble, R. Frouin, H. Grassl, B. M. Herman, M. D. King, and P. M. Teillet, "Passive remote sensing of tropospheric aerosol and atmospheric correction for the aerosol effect," J. Geophys. Res. **102,** 16815–16830 (1997).
4. M. King, Y. Kaufman, D. Tanré, and T. Nakajima, "Remote sensing of tropospheric aerosols from space: past, present, and future," AMS Bull. **80,** 2229–2259 (1999).
5. D. L. Hartmann and P. Mouginis-Mark, "Volcanoes and climate effects of aerosol," in *EOS Science Plan*, M. King, ed. (1999) (http://eospso.gsfc.nasa.gov/sci_plan/chapters.html).
6. B. Sen, G. C. Toon, J.-F. Blavier, E. L. Fleming, and C. H. Jackman, "Balloon-borne observations of mid-latitude fluorine abundances," J. Geophys. Res. **101,** 9045–9054 (1996).
7. B. Sen, G. C. Toon, G. B. Osterman, J.-F. Blavier, J. J. Margitan, R. J. Salawitch, and G. K. Yue, "Measurements of reactive nitrogen in the stratosphere," J. Geophys. Res. **103,** 3571–3585 (1998).
8. M. Carlotti, "Global-fit approach to the analysis of limb-scanning atmospheric measurements," Appl. Opt. **27,** 3250–3254 (1988).
9. R. H. Norton and C. P. Rinsland, "ATMOS data processing and science analysis methods," Appl. Opt. **30,** 389–400 (1991).
10. L. R. Brown, C. B. Farmer, C. P. Rinsland, and R. Zander, "Remote sensing of the atmosphere by high resolution infrared absorption spectroscopy," in *Spectroscopy of the Earth's Atmosphere and Intersteller Medium*, K. N. Rao and A. Webers, eds. (Academic, San Diego, Calif., 1992), pp. 97–143.
11. M. R. Gunson, M. M. Abbas, M. C. Abrams, M. Allen, L. R. Brown, T. L. Brown, A. Y. Chang, A. Goldman, F. W. Irion, L. L. Lowes, E. Mahieu, G. L. Manney, H. A. Michelsen, M. J. Newchurch, C. P. Rinsland, R. J. Salawich, G. P. Stiller, G. C.

Toon, Y. L. Yung, and R. Zander, "The Atmospheric Trace Molecule Spectroscopy (ATMOS) experiment: deployment on the ATLAS Space Shuttle missions," Geophys. Res. Lett. **23,** 2333–2339 (1996).
12. G. C. Toon, "The MkIV interferometer," Opt. Photon. News **2,** 19–21 (1991).
13. P. R. Bevington, *Data Reduction and Error Analysis for the Physical Sciences* (McGraw-Hill, New York; 1969).
14. C. P. Rinsland, G. K. Yue, M. R. Gunson, R. Zander, and M. C. Abrams, "Mid-infrared extinction by sulfate aerosols from the Mt. Pinatubo eruption," J. Quant. Spectrosc. Radiat. Transfer **52**(3/4), 241–252 (1994).
15. K. F. Palmer and D. Williams, "Optical constants of sulfuric acid: application to the clouds of Venus?" Appl. Opt. **14,** 208–219 (1975).
16. R. T. Tisdale, D. L. Glandorf, M. A. Tolbert, and O. B. Toon, "Infrared optical constants of low-temperature H_2SO_4 solutions representative of stratospheric sulfate aerosols," J. Geophys. Res. **103,** 25353–25370 (1998).
17. R. F. Niedziela, M. L. Norman, R. E. Miller, and D. R. Worsnop, "Temperature- and composition-dependent infrared optical constants for sulfuric acid," Geophys. Res. Lett. **25**(24), 4477–4480 (1998).
18. D. Weis and G. E. Ewing, "Infrared spectroscopic signatures of $(NH_4)_2SO_4$ aerosols," J. Geophys. Res. **101,** 18709–18720 (1996).
19. O. B. Toon, M. A. Tolbert, B. G. Koehler, A. M. Middlebrook, and J. Jordan, "Infrared optical constants of H_2O ice, amorphous nitric acid solutions, and nitric acid hydrates," J. Geophys. Res. **102,** 25631–25654 (1994).
20. R. F. Niedziela, R. E. Miller, and D. R. Worsnop, "Temperature-dependent and frequency-dependent optical constants for nitric acid dihydrate from aerosol spectroscopy," J. Phys. Chem. A **102,** 6477–6484 (1998).
21. H. D. Downing and D. Williams, "Optical constants of water in the infrared," J. Geophys. Res. **80,** 1656–1661 (1975).
22. I. N. Sokolik, O. B. Toon, and R. W. Bergstrom, "Modeling the radiative characteristics of airborne mineral aerosols at infrared wavelengths," J. Geophys. Res. **103,** 8813–8826 (1998).
23. U. M. Biermann, B. P. Luo, and T. Peter, "Absorption spectra and optical constants of binary and ternary solutions of H_2SO_4, HNO_3, and H_2O in the mid infrared at atmospheric temperatures," J. Phys. Chem. A **104,** 783–793 (2000).
24. M. L. Clapp, R. E. Miller, and D. R. Worsnop, "Frequency-dependent optical constants of water ice obtained directly from aerosol extinction spectra," J. Phys. Chem. **99,** 6317–6326 (1995).
25. P. Yang, K. N. Liou, and W. P. Arnott, "Extinction efficiency and single-scattering albedo for laboratory and natural cirrus clouds," J. Geophys. Res. **102,** 21825–21835 (1997).
26. P. Yang and K. N. Liou, "Finite-difference time domain method for light scattering by small ice crystals in three-dimensional space," J. Opt. Soc. Am. A **13,** 2072–2085 (1996).
27. J. Goodman, K. G. Snetsinger, R. F. Pueschel, G. V. Ferry, and S. Verma, "Evolution of Pinatubo aerosol near 19-km altitude over western North America," Geophys. Res. Lett. **21,** 1129–1132 (1994).
28. V. R. Oberbeck, E. F. Danielson, K. G. Snetsinger, G. V. Ferry, W. Fong, and D. M. Hayes, "Effect of the eruption of El Chichon on stratospheric aerosol size and composition," Geophys. Res. Lett. **10,** 1021–1024 (1983).
29. R. F. Pueschel, P. B. Russell, D. A. Allen, G. V. Ferry, K. G. Snetsinger, J. M. Livingston, and S. Verma, "Physical and optical properties of the Pinatubo volcanic aerosol: aircraft observations with impactors and a Sun-tracking photometer," J. Geophys. Res. **99,** 12915–12922 (1994).
30. R. G. Grainger, A. Lambert, F. W. Taylor, J. J. Remedios, C. D. Rodgers, M. Corney, and B. J. Kerridge, "Infrared absorption by volcanic stratospheric aerosols observed by ISAMS," Geophys. Res. Lett. **21,** 1283–1286 (1993).
31. G. Echle, T. von Clarmann, and H. Oelhaf, "Optical and micrphysical parameters of the Mt. Pinatubo aerosol as determined from MIPAS-B mid-IR limb emission spectra," J. Geophys. Res. **103,** 19193–19211 (1998).
32. H. M. Steele and P. Hamill, "Effects of temperature and humidity on the growth and optical properties of sulfuric acid–water droplets in the stratosphere," J. Aerosol Sci. **12,** 517–528 (1981).
33. J. H. Seinfeld and S. N. Pandis, *Atmospheric Chemistry and Physics* (Interscience, New York, 1998), pp. 429–440.
34. O. B. Toon, J. B. Pollack, and B. N. Khare, "The optical constants of several atmospheric aerosol species: ammonium sulfate, aluminum oxide, and sodium chloride," J. Geophys. Res. **81,** 5733–5748 (1976).
35. G. D'Almeida, "On the variability of desert aerosol radiative characteristics," J. Geophys. Res. **92,** 3017–3026 (1987).
36. C. P. Rinsland, M. R. Gunson, P.-H. Wang, R. F. Arduini, B. A. Baum, P. Minnis, A. Goldman, M. C. Abrams, R. Zander, E. Mahieu, R. J. Salawitch, H. A. Michelson, F. W. Irion, and M. J. Newchurch, "ATMOS/ATLAS-3 infrared profile measurements of clouds in the tropical and subtropical upper troposphere," J. Quant. Spectrosc. Radiat. Transfer **60,** 903–919 (1998).
37. A. Lambert, R. G. Grainger, C. D. Rodgers, F. W. Taylor, J. L. Mergenthaler, J. B. Kumer, and S. T. Massie, "Global evolution of the Mt. Pinatubo volcanic aerosols observed by the infrared limb-sounding instruments CLAES and ISAMS on the Upper Atmosphere Research Satellite," J. Geophys. Res. **102,** 1495–1512 (1997).
38. R. G. Grainger, A. Lambert, C. D. Rodgers, F. W. Taylor, and T. Deshler, "Stratospheric aerosol effective radius, surface area, and volume estimated from infrared measurements," J. Geophys. Res. **100,** 16507–16518 (1995).
39. L. W. Thomason, L. R. Poole, and T. Deshler, "A global climatology of stratospheric aerosol surface area density deduced from Stratospheric Aerosol and Gas Experiment II measurements: 1984–1994," J. Geophys. Res. **102,** 8967–8976 (1997).